Molecular Dynamics and X-Ray Diffraction Study of Aqueous Beryllium(II) Chloride Solutions

T. Yamaguchi, H. Ohtaki
Department of Electronic Chemistry, Tokyo Institute of Technology, Nagatsuta, Midori-ku, Yokohama 227, Japan

E. Spohr, G. Pálinkás, K. Heinzinger
Max-Planck-Institut für Chemie (Otto-Hahn-Institut), D-6500 Mainz, FRG

M. M. Probst
Institut für Anorganische und Analytische Chemie, Universität Innsbruck, A-6020 Innsbruck, Austria

Z. Naturforsch. **41 a,** 1175–1185 (1986); received July 14, 1986

A structural investigation of a 1.1 molal $BeCl_2$ aqueous solution has been performed by a molecular dynamics simulation together with X-ray diffraction studies of 1.1 and 5.3 molal $BeCl_2$ aqueous solutions at pH = 1. A central force model in combination with an improved intramolecular three-body potential was used for water. The ion-water and ion-ion potentials were derived from *ab initio* calculations. The structure function obtained from the simulation is in satisfactory agreement with that from X-ray diffraction. The MD simulation of the 1.1 molal solution shows that the hydration shell of Be^{2+} consists of six water molecules occupying octahedral sites around a central Be^{2+}. The X-ray scattering data of the 5.3 molal solution indicate that Be^{2+} has only four water molecules in the first hydration shell. The average coordination number of Cl^- is found to be about seven in the 1.1 molal solution from both X-ray diffraction and MD simulation, but Cl^- is surrounded on the average by 3.4 water molecules in the 5.3 molal solution. The influence of the small divalent Be^{2+} on the geometry of its nearest neighbour water molecules is compared with the results of previous simulations of 1.1 molal $MgCl_2$ and $CaCl_2$ solutions.

1. Introduction

Molecular dynamics (MD) simulations in conjunction with X-ray and neutron diffraction experiments have successfully elucidated the structural (especially the hydration shell structure of ions) and dynamic properties of aqueous alkali halide solutions [1]. Recently, MD simulations have also been applied to aqueous solutions involving doubly charged ions like Mg^{2+} [2, 3] and Ca^{2+} [4a]. The results have demonstrated that Mg^{2+} has a strongly preferred octahedral arrangement of the water molecules in the first hydration shell, whereas the larger Ca^{2+} tends to have about nine nearest-neighbour water molecules arranged in a none-regular way [4b]. For a comparison with these divalent ions, it is of interest to examine the hydration phenomenon of the smaller Be^{2+} in aqueous solutions.

The structure of Be(II) hydrates in the solid state has been established from X-ray [5] and neutron [6] diffraction studies and from infrared and Raman spectra [7] to consist of four water molecules, forming a tetrahedron with a slight angular distortion of the T_d symmetry. No direct structural information of the hydrated Be^{2+} in aqueous solutions is available so far but a hydration number of four has been concluded from several NMR measurements [8–11]. Infrared and Raman spectra of beryllium(II) hydrates in aqueous solutions have shown an intense, strongly polarized band around 530 cm^{-1} and weaker depolarized peaks at 880 and 355 cm^{-1}, which were assigned, respectively, to the ν_1, ν_3 and ν_4 modes of the tetrahedral $Be(OH_2)_4^{2+}$ ion, but the spectra are complicated by the presence of extra peaks due to hydrolysis products [12–15]. As no diffraction work on aqueous solutions containing Be^{2+} ions has been performed so far, it is one of the aims of the present investigation to determine the hydration number of Be^{2+} and to examine the geometrical arrangement of the water molecules in the first coordination shell.

Reprint requests to Prof. H. Ohtaki, Department of Electronic Chemistry, Tokyo Institute of Technology, Nagatsuta, Midori-ku, Yokohama 227, Japan.

0340-4811 / 86 / 1000-1175 $ 01.30/0. – Please order a reprint rather than making your own copy.

In order to check the consistency between experiments and MD simulations, an X-ray scattering measurement of an aqueous 1.1 molal $BeCl_2$ solution was performed with a slight excess of H^+ ions because Be^{2+} hydrolyses to form polynuclear species $Be_3(OH)_3^{3+}$ and $Be_2(OH)^{3+}$ at higher *p*H [16, 17]. In addition, a 5.3 molal $BeCl_2$ solution was measured in order to emphasize the interactions within the hydration structure of Be^{2+} having small X-ray scattering amplitudes.

2. Pair Potentials and Details of the Simulation

All intermolecular potentials in the simulation presented here were of pair potential type and consisted of a Coulomb part for which the Ewald summation was applied and of short range parts for which the shifted force method was used [18].

Water was described by a model which treated the intermolecular O−O, O−H, and H−H interactions by means of the latest version of the central force (CF2) model [19] but used a three-body potential for a more correct description of the intramolecular interactions [20, 21]. This modification has led to a marked improvement with respect to the intramolecular vibrational motions and the dissociation energy of the water molecules. As the intermolecular part of the potential is very similar to the one employed in previous work, a direct comparison is thus possible, e.g., with the results of the $MgCl_2$ and $CaCl_2$ simulations [2−4].

The pair potentials for $Be^{2+}-O$, $Be^{2+}-H$, $Be^{2+}-Be^{2+}$, and $Be^{2+}-Cl^-$ were derived from new Hartree Fock calculations. It is known that for such systems the electron correlation does not contribute significantly to the binding energy [22]. The Dunning GTO double zeta valence basis set [23] was used, which was augmented by polarization functions. Altogether, we calculated several hundred energy points. The Hartree Fock energies were in excellent agreement with the calculations of Corongiu and Clementi [24] (where the energies for a smaller number of different orientations were calculated) as well as with the calculation of the energy minimum of Kollmann and Kuntz [25]. Since the CF2 water is flexible, it is not guaranteed that potentials obtained from calculations with rigid water do not introduce force that lead to an artificial distortion of the water. To overcome this problem we calculated our energies not only with the water in the CF2 equilibrium geometry but also for different HOH angles. To obtain simple analytical expressions, we fitted three-parameter functions for the Be−O and Be−H interactions toward the *ab initio* energies after subtracting from them the Coulombic contributions that were already determined by the CF2 model and the charges of the ions. In a similar way we obtained the potentials for the $Be^{2+}-Be^{2+}$ and $Be^{2+}-Cl^-$ interactions. The potentials involving Be^{2+} are shown in Table 1, together with the other ones used in [2] and [4]. Figure 1 shows the *ab initio* energies and the fitted potentials for the ion-water orientation with C_{2v} symmetry and the water molecules in equilibrium geometry, where the global energy minimum is found.

Table 1. Pair potentials employed in the simulation. Energies are given in 10^{-19} J and distances in Å. For intramolecular potentials see [20]. The cutoff distances in units of the side length of the box were 0.45, 0.22 and 0.16 for $V_{OO}(r)$, $V_{OH}(r)$, and $V_{HH}(r)$, respectively, and 0.5 for all others.

$$
\begin{aligned}
V_{OO}(r) &= 10.04/r + 1858/r^{8.86} - 0.01736/\\
&\quad \cdot \{\exp[-4(r-3.4)^2] + \exp[-1.5(r-4.5)^2]\}\\
V_{OH}(r) &= -5.019/r + 0.433/r^{9.2}\\
&\quad - 0.694/\{1 + \exp[40(r-1.05)]\}\\
&\quad - 0.278/\{1 + \exp[5.493(r-2.2)]\}\\
V_{HH}(r) &= 2.509/r + 6.957/\{1 + \exp[29.9(r-1.968)]\}\\
V_{BeO}(r) &= -30.43/r - 23.03/r^2 + 1719\exp(-3.78r)\\
V_{BeH}(r) &= 15.22/r + 1.037/r^2 + 0.495\exp(-0.0859r)\\
V_{BeBe}(r) &= 92.27/r - 3.534/r^2 + 1.994\exp(-0.628r)\\
V_{BeCl}(r) &= -46.14/r - 1.033/r^2 + 15855\exp(-4.77r)\\
V_{ClO}(r) &= 15.22/r - 1.849/r^2 + 6304\exp(-3.21r)\\
V_{ClH}(r) &= -7.609/r + 3.138\times 10^{24}\exp(-34r)\\
V_{ClCl}(r) &= 23.07/r + 476.1/r^6 + 15230\exp(-3.39r)
\end{aligned}
$$

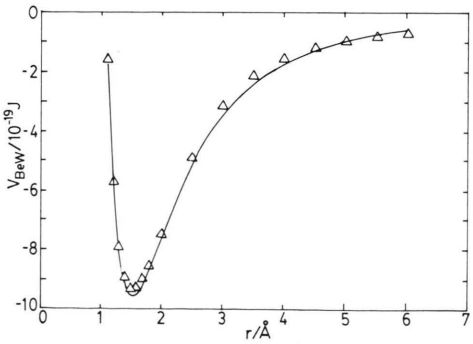

Fig. 1. Beryllium-water potential for C_{2v} geometry with an HOH angle of 104.52°. Triangles indicate energy values from the *ab initio* calculations.

The basic cube contained 200 water molecules, 4 cations, and 8 anions representing a 1.1 molal $BeCl_2$ solution. A side length of the cube of 18.33 Å was calculated from the experimental density at 25 °C of 1.051 g/cm^3 for a 1.1 molal $BeCl_2$ aqueous solution with $p\mathrm{H} = 1$ as used in subsequent X-ray measurements. After several thousand time steps of equilibration the collection of data was started. The simulation was performed for about 4000 time steps of 0.25 fs each without rescaling, leading to a total elapsed time of about 1 ps. The average temperature of the system was 310 K. The total energy was stable to better than 0.01% during the whole run.

3. X-Ray Scattering

The 1.1 and 5.3 molal aqueous solutions used for the X-ray measurements were prepared by dissolving a weighed amount of $BeCl_2$ (99.5%) into a 0.1 mol/dm^3 aqueous HCl solutions to prevent hydrolysis of Be^{2+}. The densities of the solutions were measured pychnometrically to be 1.051 and 1.227 g/cm^3 for the 1.1 and 5.3 molal solutions, respectively.

The X-ray scattering measurements of the solutions were performed at 25 °C using a $\theta-\theta$ diffractometer with Mo$K\alpha$ radiation ($\lambda = 0.7107$ Å). A graphite crystal was used for monochromatization of the scattered X-rays. The measurements were extended over the range $1° \leqq \theta \leqq 70°$ (2θ is the scattering angle), corresponding to the range

$$0.03\ \text{Å}^{-1} \leqq s \leqq 15.5\ \text{Å}^{-1}\ \ (s = 4\pi \sin\theta/\lambda)\,.$$

The scattered intensities were collected with 80 000 impulses at each data point. Details of the diffractometer and the measurements have previously been described [26]. The corrections for background, absorption, polarization, multiple scattering, and incoherent scattering, and then scaling of the corrected intensities to the absolute unit intensities were made in the usual manner [26, 27].

The experimental structure function is given by

$$i_{\mathrm{exp}}(s) = [I(s) - \sum x_\alpha f_\alpha^2(s)]/[\sum x_\alpha f_\alpha(s)]^2, \quad (1)$$

where $I(s)$ is the corrected absolute coherent intensity, x_α the mole fraction and $f_\alpha(s)$ the scattering factor of atom α. The experimental radial distribution function has been calculated from the si(s) values *via* Fourier transformation:

$$G(r) = 1 + (2\pi^2 \varrho_0 r)^{-1} \int_0^{s_{\max}} \mathrm{si}(s)\, M(s) \sin(sr)\, \mathrm{d}s\,, \quad (2)$$

where ϱ_0 is the number density of the sample, $s_{\max}$ a maximum value of s attained in the experiments, and $M(s) = \exp(-0.01\, s^2)$ the damping factor used to eliminate the truncation error in the Fourier transform and to minimize the uncertainties in the structure function at high s.

A theoretical structure function based on a model has been obtained according to

$$\begin{aligned} i(k)_{\mathrm{syn}} = {} & (\sum x_\alpha f_\alpha)^{-2} \sum\sum x_\alpha n_{\alpha\beta} f_\alpha f_\beta \sin(sr_{\alpha\beta})/(sr_{\alpha\beta}) \\ & \cdot \exp(-b_{\alpha\beta} s^2) - \sum\sum x_\alpha x_\beta f_\alpha f_\beta (4\pi R_\alpha^3/V) \\ & \cdot [\sin(sR_\alpha) - sR_\alpha \cos(sR_\alpha)]/(sR_\alpha)^3 \exp(-B_\alpha s^2)\,, \end{aligned} \quad (3)$$

where $r_{\alpha\beta}$ is the interatomic distance, $b_{\alpha\beta}$ the temperature factor, which is related to the root mean square deviation (rmsd, l) by $b = l^2/2$, and $n_{\alpha\beta}$ the number of interactions of discrete structures. Beyond these distances an uniform electron distribution was assumed. R_α and B_α are the radius of the spherical hole around atom α and the sharpness parameter of the emergence of the continuum, respectively. The correction of the anomalous dispersion was made for all atoms. The scattering factors of the neutral atoms and the values of the anomalous dispersion were taken from [28]. All calculations were carried out by means of the program KURVLR [29].

4. Results and Discussion

4.1. Radial Pair Distribution Functions from the MD Simulations

Figure 2 shows the ion-oxygen and ion-hydrogen radial distribution functions (RDFs) and the corresponding running integration numbers defined by

$$n_{\alpha\beta}(r) = 4\pi \varrho_\beta \int_0^r g_{\alpha\beta}(r')\, r'^2\, \mathrm{d}r'\,, \quad (4)$$

where ϱ_β is the number density of species β. Table 2 gives the characteristic values of the $g_{\alpha\beta}(r)$'s. In $g_{\mathrm{BeO}}(r)$ the first sharp peak due to the strong Be^{2+}-water interactions in the first hydration shell is observed at 1.75 Å, a distance longer by 0.1 Å than

Table 2. Characteristic values for the radial distribution functions $g_{\alpha\beta}(r)$. R_i, r_{Mi}, and r_{mi} are the distances in Å where for the ith time $g_{\alpha\beta}$ is unity, has a maximum and a minimum, respectively. For O–H and H–H only intermolecular data are given.

α	β	R_1	r_{M1}	$g_{\alpha\beta}(r_{M1})$	R_2	r_{m1}	$g_{\alpha\beta}(r_{m1})$	$n_{\alpha\beta}(r_{m1})$	r_{M2}	$g_{\alpha\beta}(r_{M2})$
Be	O	1.62	1.75	25.5	2.01	2.35–2.43	≅ 0.0	6.0	3.73	3.22
Be	H	2.23	2.49	7.50	2.76	2.95	0.47	12.7	4.59	2.15
Cl	O	2.93	3.12	2.56	3.68	3.93	0.63	7.4	–	–
Cl	H	1.99	2.25	2.28	2.59	2.60	0.56	6.1	3.50	1.28
O	O	2.44	2.80	2.99	3.20	3.3	0.91	5.4	4.85	1.25
O	H	1.72	1.97	1.22	2.31	2.40	≅ 0.5	4.0	3.16	1.61
H	H	2.14	2.28	1.82	2.85	3.05	0.88	7.4	≅ 3.7	1.11

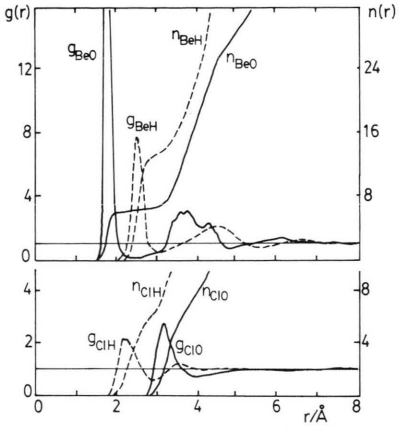

Fig. 2. Ion-oxygen and ion-hydrogen radial distribution functions and running integration numbers for the 1.1 molal $BeCl_2$ solution.

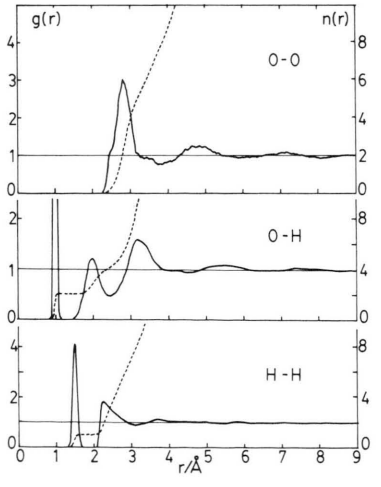

Fig. 3. Oxygen-oxygen, oxygen-hydrogen, and hydrogen-hydrogen radial distribution functions (full) and running integration numbers (dashed) for the 1.1 molal $BeCl_2$ solution.

known from the crystal structure of $BeSO_4 \cdot 4H_2O$ [5, 6]. The peak (25.5) is higher than the corresponding ones for Mg^{2+} (19.2) and Ca^{2+} (14.0), which indicates an even more pronounced hydration shell of Be^{2+} than those of Mg^{2+} and Ca^{2+}. The second hydration shell of Be^{2+} is observed at 3–5 Å and is clearly separated from the first shell, this feature being similar to those found for Mg^{2+} and Ca^{2+}. An unexpected result is the coordination number of Be^{2+}, $n(r_{m1}) = 6$, contrary to the value of four reported previously from NMR measurements. This will be discussed in a later section.

The first Be–H peak appears at 2.49 Å, compared with 2.75 Å and 3.13 Å for Mg^{2+}–H and Ca^{2+}–H, respectively. This is in accordance with the shifts of the first ion-oxygen peaks from 1.75 Å to 2.00 Å and 2.39 Å. The height of the peak increase by 1.5 from those for Mg^{2+} (5.96) and Ca^{2+} (5.98), indicating a more rigid conformation of coordinated water molecules for Be^{2+} than for Mg^{2+} and Ca^{2+}. The $n_{BeH}(r_{m1})$ value is similar to that for Mg^{2+} (12.5) but smaller than that for Ca^{2+} (18.7). This is simply because of the average coordination number of six for both Be^{2+} and Mg^{2+} and 9.2 for Ca^{2+}. The $n_{BeH}(r_{m1})$ value of 12.7 corresponds to the hydrogen atoms all belonging to the six water molecules found in the first hydration shell of Be^{2+}.

The first neighbour Cl–O distance observed is slightly shorter than those seen in the $MgCl_2$ (3.18 Å) and $CaCl_2$ solutions (3.19 Å), while the heights of the first peaks in $g_{ClO}(r)$ and $g_{ClH}(r)$ decrease with increasing cation size. The Cl–H distance is very similar for the three solutions. The second hydration shell of Cl^- is not observed in the $BeCl_2$ solution. The $n_{ClO}(r_m)$ value is in between those obtained for the $MgCl_2$ (7.0) and $CaCl_2$ (7.9) solutions.

Figure 3 shows the O−O, O−H, and H−H RDFs and the corresponding running integration numbers. The $g_{OO}(r)$ for the $BeCl_2$ solution shows two shoulders around 2.5 and 3.5 Å, which have not been observed for the $MgCl_2$ and $CaCl_2$ solutions. These characteristic shoulders have been found to correspond to *cis* and *trans* O−O distances within the octahedral hydration shell of Be^{2+} as discussed in a later section. Another noteworthy feature of the $g_{OO}(r)$ is a shallow minimum, compared with those for the $MgCl_2$ (0.75) and $CaCl_2$ (0.80) solutions. This together with a slight decrease of the height of the first peak indicates a stronger disturbance of the water structure by Be^{2+} when compared with Ca^{2+} and Mg^{2+} (see Fig. 10 below). There seem to be no significant differences for $BeCl_2$, $MgCl_2$ and $CaCl_2$ as far as $g_{OH}(r)$ and $g_{HH}(r)$ are concerned except for the less deep first minimum in $g_{OH}(r)$ in the $BeCl_2$ solution which again could mean poorer hydrogen bonding.

4.2. *X-Ray Scattering Results*

Experimental structure functions and total radial distribution functions of the 1.1 and 5.3 molal $BeCl_2$ aqueous solutions are shown in Figs. 4 and 5, respectively, together with those obtained from the MD simulation of the 1.1 molal solution.

In the structure function of the 1.1 molal solution, a discrepancy between experiment and simulation is observed in the range 2−3 $Å^{-1}$, i.e. a lower shoulder at 2.2 $Å^{-1}$ and a higher first peak at 3 $Å^{-1}$ in the simulated si(s), which has also been seen in previous simulations of the $MgCl_2$ and $CaCl_2$ solutions. The discrepancy may originate from the water-water interactions as demonstrated in the corresponding partial structure function for the $MgCl_2$ solution which has shown a similar discrepancy for the same s values [3]. At $s > 12$ $Å^{-1}$ the experimental structure function of the 1.1 molal solution is noisy, indicating a small contribution of the structure of the solution of the si(s) function as seen in the simulated one.

In the total radial distribution function of the 1.1 molal solution obtained from the simulation, a small peak due to the Be−O interactions appears at 1.7 Å. However, the experimental $G(r)$ function showed no appreciable peak but small ripples in the corresponding r range, which was caused probably by random errors in the experimental structure function at high s. In the 5.3 molal solution, a peak due to the Be−O interactions is clearly visible at 1.65 Å.

The distinct peak at 2.9 Å for the 1.1 molal solution is assigned mainly to the first neighbour O−O distances in the bulk [30] and in part to the Cl−O interactions due to the anionic hydration [2−4]. With increasing solute concentration the peak shifts to 3.2 Å because the Cl−O interactions predominate in the 5.3 molal solution. A shoulder left around 2.6 Å in $G(r)$ for the 5.3 molal solution may be ascribed to the interactions between water molecules within the first hydration shell of Be^{2+}.

On the basis of the above assignment of the peaks in the $G(r)$ functions, we analysed the structure functions quantitatively by using a least-squares

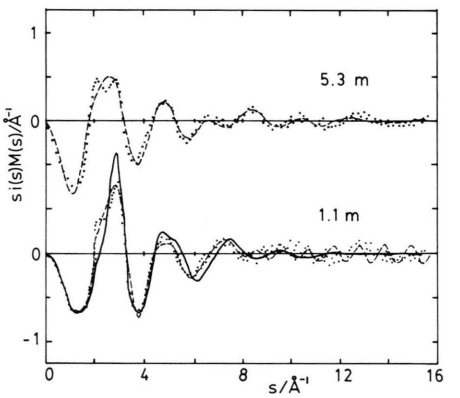

Fig. 4. X-Ray structure functions from experiment (dots), a model fit (dashed), and the MD simulation (full) for the 1.1 and 5.3 molal $BeCl_2$ solutions.

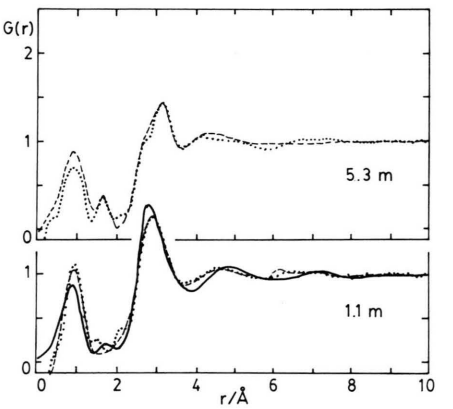

Fig. 5. Total radial distribution functions from experiment (dots), a model fit (dashed) and the MD simulation (full) for the 1.1 and 5.3 molal $BeCl_2$ solutions.

fitting procedure in which a minimum of the function

$$U = \sum_{s_{min}}^{s_{max}} w(s)\,[i(s)_{exp} - i(s)_{syn}]^2, \qquad (5)$$

was searched by program NLPLSQ [31] with variables r, b, n, R, and B in (3). s_{min} and s_{max} are the lower and upper limits of s used in the fits, and $w(s)$ is a weighting function proportional to s^4.

The adopted model had the following characteristics:

a) The hydration shell structure of Be^{2+} is discrete as in $Be(OH_2)_n^{2+}$. The Be–O and O–O interactions were taken into account by introducing the parameters r_{BeO}, b_{BeO}, n_{BeO}, r_{OO}, b_{OO} and n_{OO}, of which r_{OO} and n_{OO} follow from the assumed geometry: $n_{BeO} = 4$ for the tetrahedral model A and 6 for the octahedral model B. The contribution of the hydrated Be^{2+} ion was not included in the fits of the X-ray data for the 1.1 molal solution because it was negligibly small in the si(s) values. Indeed the fits with or without its contribution gave similar U values.

b) The structure of the hydrated Cl^- was expressed in terms of the parameters r_{ClO}, b_{ClO}, and n_{ClO}, which were allowed to vary independently. The water-water interactions within the hydration shell of Cl^- were not included because of no strong correlation between them as revealed in [3].

c) Be^{2+}–Cl^- contacts were assumed for the 5.3 molal solution since the formation of cationic complexes was plausible in concentrated $BeCl_2$ solutions [32]. The Be–Cl distance was expected to be about 2.1 Å from the sum of the ionic radii of Be^{2+} and Cl^- [33]. The experimental $G(r)$ showed a small hump at the corresponding distance. The parameters r_{BeCl}, b_{BeCl}, and n_{BeCl} were allowed to vary independently.

d) The water-water interactions were divided into two kinds: (i) those from the bulk structure present in a 1.1 molal solution, in which the pentamer structure proposed from many previous works [30, 34] was assumed, (ii) those from the interactions between coordinated water molecules in the first and second hydration shells. This treatment seemed reasonable since the latter hydrogen bonds give shorter distance than the former ones [3].

e) Beyond the above discrete structures, a uniform electron distribution was assumed for each atom.

The final results are summarized in Table 3. The si(s) and $G(r)$ functions calculated using the parameter values in Table 3 (Model A for the 5.3 molal solution) are compared with the experimental ones in Figs. 4 and 5, respectively. The present model has well reproduced the observed values. From the R-value, model A is preferred for the 5.3 molal solution. Apparently, the rmsd for the Be–O interactions obtained in model B is too large and in model A too small. The fits including the Be^{2+}–Cl^- interactions did not improve the R-value significantly. This may be due partly to the small X-ray scattering amplitude of Be and probably to a small amount of the Be^{2+}–Cl^- contacts formed in the 5.3 molal solution. In Fig. 5 (above), the discrepancy between the experiment and the fit around 2 Å is within the uncertainties.

4.3. *Properties of the Hydration Shell of Be^{2+}*

From the knowledge of the position of all particles as a function of time, provided by the MD simulation, the geometrical arrangement of the

Table 3. Structure parameters obtained from least-squares fits for the X-ray data of the 1.1 and 5.3 molal $BeCl_2$ aqueous solutions; interatomic distance r(Å), the root mean square deviation l(Å), and the number of interactions N. Models A and B correspond to four- and six-fold coordination models for Be^{2+}, respectively.

		1.1 m	5.3 m	
			A	B
$Be(OH_2)_N^{2+}$	r_{BeO}		1.67	1.66
	l_{BeO}		0.035	0.14
	N_{BeO}		4[a]	6[a]
	l_{OO}		0.23	0.28
$Cl(H_2O)_N^-$	r_{ClO}	3.24	3.15	3.15
	l_{ClO}	0.21	0.17	0.17
	N_{ClO}	6.9	3.5	3.7
H_2O–H_2O[b]	r_{OO}	2.76	2.71	2.77
	l_{OO}	0.31	0.19	0.17
	N_{OO}[c]	1.2	1.1	1.1
bulk	r_{OO}	2.82	–	–
H_2O–H_2O[d]	l_{OO}	0.21	–	–
	l'_{OO}	0.54	–	–
Fit s-range/Å^{-1}		0.8–12.0	0.2–15.0	0.2–15.0
R[e]		0.181	0.252	0.381

[a] Fixed. [b] Interactions between water molecules in the first and second coordination shells. [c] Per H_2O molecules coordinated. [d] Pentamer structure of free water molecules was assumed. l_{OO} and l'_{OO} represent the rmsd's of the first and the second neighbour O–O interactions in the bulk, respectively. [e] $R = [\sum w(s)\{i_{exp}(s) - i_{syn}(s)\}^2 / \{\sum w(s)\, i_{exp}(s)\}^2]^{1/2}$.

water molecules in the first hydration shell of Be^{2+} has been deduced. In order to achieve this aim a coordinate system has been introduced where the ion defines the origin, one oxygen atom of the hydration shell water molecules the z-axis and a second one the xz-plane. The projection of the oxygen atom positions of the six nearest neighbour water molecules around Be^{2+}-collected at several hundred different times spread over the whole simulation – onto the xy-plane of this coordinate system are shown in Fig. 6 in the form of a three-dimensional drawing. Figure 6 shows unambiguously that they are arranged octahedrally with practically no distortion and a narrow distribution around the octahedral positions. The result is very similar to what has been found for Mg^{2+} [3].

Although there is no significant difference between Mg^{2+} and Be^{2+} as far as the average geometrical arrangement of the water molecules in the first hydration shell of both ions is concerned, they differ in the answer to the question how many water molecules occupy octahedral positions at the same time. In order to derive this information from the simulation, solid angles have to be defined on the basis of which it is decided if the oxygen atom of a given water molecule occupies an octahedral position. In the choice of these angles there is, of course, some arbitrariness involved. It was decided to choose a solid angle of 0.12π centred at each of the octahedral directions, corresponding to an aperture angle of each cone of 40°. The percentage of simultaneous occupation of all six octahedral positions has been calculated from the simulation to be 74 for Be^{2+} and 61 for Mg^{2+}, while the average number of simultaneously occupied octahedral positions is 5.5 and 5.1, respectively. This is just a consequence of the stronger interactions of the smaller Be^{2+} with its first shell water molecules.

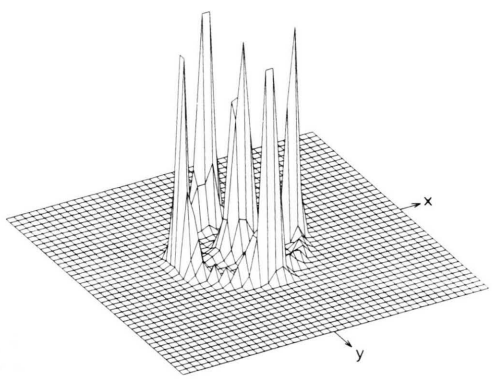

Fig. 6. Three-dimensional drawing of the projection of the oxygen atom positions of the six nearest neighbour water molecules around a Be^{2+} onto the xy-plane of a coordinate system defined in the text.

The structural parameters of the hydration shell of Be^{2+} obtained from the MD simulation and the X-ray diffraction are given in Table 4, together with previous results from other methods. The Be–O distance obtained from the present X-ray measurements is appreciably longer than those found in the crystal structure of $BeSO_4 \cdot H_2O$. The simulation gives an even longer Be–O distance than the X-ray measurement of the 5.3 molal solution, which has certainly to be ascribed to the higher coordination number of six. Previous NMR, infrared and Raman spectra have all indicated about four as the average hydration number of Be^{2+} in aqueous solutions. The present X-ray scattering data of the 5.3 molal solution also give a coordination number of four. Unfortunately, the scattering power of Be^{2+} for X-rays is very small and therefore a coordination number could not be deduced from the X-ray measurement of the 1.1 molal $BeCl_2$ solution.

The two main reasons why the simulation might give a different hydration number are the starting configuration and the pair potentials employed. Because of the strong Be^{2+}-water interaction the residence time of the water molecules in the first hydration shell of Be^{2+} is by a few orders of magnitude longer than the simulation time. This means, of course, if at the beginning 6 water molecules are in the first shell there will not be time enough for them to leave. In order to rule out this point several

Table 4. Comparison of the structural parameters for the hydration shell of Be^{2+} obtained from various methods. r is the Be–O distance and N the hydration number.

r/Å	N	Molality	Method	Ref.
1.610	4		X-ray[a]	[5]
1.618	4		neutron[a]	[6]
–	4.0–4.3	3[b]	NMR	[8]
–	3.7–3.9	1.02–3.17	NMR	[9]
–	4.0	1.500	NMR	[10]
–	4.5	2.70[b]	NMR	[11]
1.67	4	5.3	X-ray	This work
1.75	6.0	1.1	MD	This work

[a] In crystals. [b] mol/dm^3.

preliminary runs have been made with starting configurations where only four water molecules were positioned in the immediate neighbourhood of Be^{2+}. In each case after less than 0.5 ps a hydration number of six resulted.

With decreasing ion size the polarization of the water molecules in the hydration shell and charge transfer effects make the asssumption of pair additivity of the potentials more questionable. These effects tend to decrease the hydration number, however a very rough estimate seems to indicate that they are not sufficient to decrease the hydration number of Be^{2+} from six to four.

In conclusion it can be stated that the hydration number of Be^{2+} in moderately dilute aqueous solutions remains undecided. Spectroscopic measurements are not the most reliable way to determine hydration numbers. Diffraction data at low concentrations do not give definite answers, and the potentials employed in the simulation need to be improved by including many-body interactions. The situation is similar to that of Li^+ which was examined about ten years ago, though Li^+ does not hydrolyse but Be^{2+} does at higher *p*H. Different from what had been concluded from experiments, the MD simulation predicted for Li^+ a hydration number of six instead of four [35], which was later confirmed by neutron diffraction measurements with isotopic substitution [36].

4.4. *Hydration Shell of Cl^-*

The Cl−O distance obtained from the present X-ray measurement for the 1.1 molal solution (3.24 Å, Table 3) agrees with that from the MD simulation (3.12 Å, Table 2) within the experimental uncertainties. The rmsd of 0.2 Å is within accepted values for the uncertainties. For the 1.1 molal solution, the average coordination number of Cl^- obtained from the X-ray study is consistent with that derived from the MD simulation. The calculation of the average geometrical arrangement of the water molecules in the first hydration shell of Cl^- from the simulation (as shown for Be^{2+} in Fig. 6) gives a uniform distribution. This result has been found before for other chloride solutions, too (see e.g. [1]).

The X-ray measurement of the 5.3 molal solution leads to a very small coordination number of Cl^- of 3.4 although the Cl^-−O distance and its rmsd are very similar to those for the 1.1 molal solution. A small hydration number of Cl^- (3.9) has also been found from a neutron diffraction study with isotopic substitution of a 2.85 molal $NdCl_3$ solution [38]. The first-order-difference method of neutron diffraction studies of aqueous 3.57 and 9.95 molal LiCl solutions [36] revealed the hydration number of Cl^- to be 5.9 and 5.3, respectively. Moreover, the hydration number of Cl^- further decreases to 4.4 in a 14.9 molal LiCl solution, in which a direct contact Li^+−Cl^- species is formed, as revealed by the second-order-difference method [39]. Thus, from the diffraction measurement, the decrease in the hydration number of Cl^- in the 5.3 molal $BeCl_2$ solution could not be explained until the ion-ion pair distribution functions were derived from the second-order-difference method. An MD simulation at higher concentration might help to understand the structural changes leading to this small number.

4.5. *Average Interaction Energies*

Figure 7 shows the average interaction energy between a water molecule and the central ion as a function of the ion-O distance. For Be^{2+}, contrary to the $MgCl_2$ solution, an unexpected feature is found, which shows that the position of the minimum in the average potential energy has shifted to 1.7 Å, a distance longer than that in the corresponding pair potential (1.55 Å), which was not the case in the $MgCl_2$ and $CaCl_2$ solutions. This may be caused by a stronger water-water repulsion within the smaller

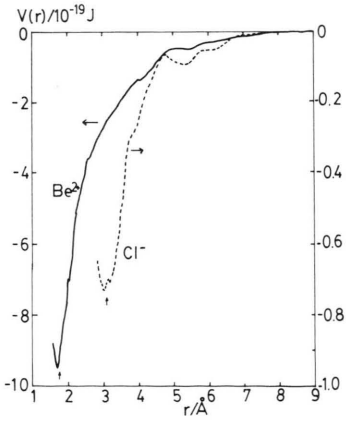

Fig. 7. Average potential energy of a water molecule with respect to Be^{2+} and Cl^- as a function of ion-oxygen distance. The positions of the maxima in the RDFs are marked by an arrow.

hydration shell of Be^{2+} than that in the case of Mg^{2+}. The position of the minimum is close to that of the first peak in the $g_{BeO}(r)$.

The average potential energy of Cl^- has a minimum around 3.2 Å, at which the first peak has been observed in $g_{ClO}(r)$ (Figure 7). This feature is consistent with that found in the $MgCl_2$ and $CaCl_2$ solutions.

Figure 8 shows the average water-water potential energy as a function of O–O distance. A characteristic feature of the potential is a steep positive part below 2.6 Å and a positive hump at 3.2–4.1 Å. They correspond to similar features in $g_{OO}(r)$ (Fig. 3) and arise from *cis* and *trans* H_2O-H_2O within the octahedrally hydrated Be^{2+}. Thus, the large charge density on the Be^{2+} forces coordinated water molecules to orient in an energetically unfavourable way relative to each other. A similar feature of the water-water potential energy has been observed in the MD simulation of an $LiCl_4 \cdot 4H_2O$ solution, in which all the water molecules are bonded to the ions [37].

4.6. *Orientation of the Water Molecules*

The distribution of $\cos\theta$ for the water molecules in the first hydration shells of Be^{2+} and Cl^- is compared in Fig. 9 with the results of the simulations of 1.1 molal $MgCl_2$ and $CaCl_2$ solutions [2, 4]. θ is defined as the angle between the dipole moment direction of the water molecule and the vector pointing from the oxygen atom towards the center of the ion. For all three cations a trigonal orientation is found and the distributions are quite similar. Preferentially linear hydrogen bonds are formed between Cl^- and the water molecules in its first hydration shell. The differences in the distributions for different counterions are small but seem to be significant. The sharpness of the distributions decreases with decreasing cation size indicating a stronger disturbance of the hydration shell of Cl^- by the smaller counterion.

The cations also strongly influence the hydrogen bond structure of the bulk water, as can be seen from Fig. 10 where the distributions of the hydrogen bond angles Ψ, as defined in the insertion, are shown for pure water as well as for the 1.1 molal $BeCl_2$, $MgCl_2$ and $CaCl_2$ solutions. In the case of the solutions the distributions are calculated only for bulk water, which means that the water molecule from which the angle is measured does not belong to the first hydration shells of one of the

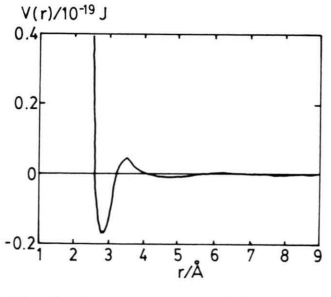

Fig. 8. Average potential energy of two water molecules as a function of oxygen-oxygen distance.

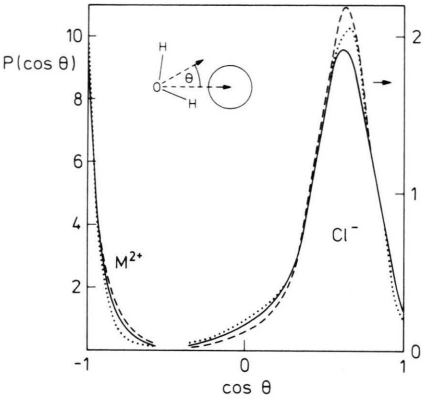

Fig. 9. Distribution of $\cos\theta$ for the water molecules in the first hydration shells of the ions from MD simulations of 1.1 molal $BeCl_2$ (full), $MgCl_2$ (dotted) and $CaCl_2$ (dashed) solutions. θ is defined in the insertion.

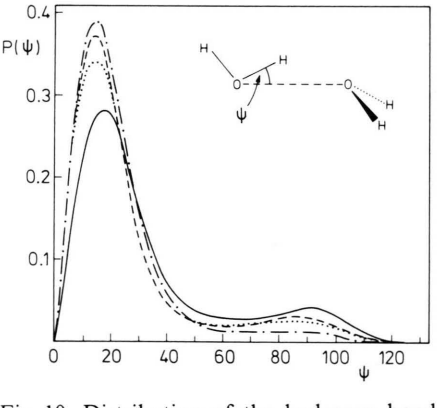

Fig. 10. Distribution of the hydrogen bond angles Ψ for pure water (dash-dotted) and the bulk water in 1.1 molal $CaCl_2$ (dashed), $MgCl_2$ (dotted) and $BeCl_2$ (full) solutions. Ψ is defined in the insertion.

ions. The disturbance of the bulk water structure strongly increases with decreasing cation size.

4.7. Geometries of the Water Molecules

The central force type model for water employed in the simulation [20] permits the investigation of the influence of the ions on the water molecule geometry. The average intramolecular distance of 0.975 Å was found to be the same for bulk water and hydration water of Cl^-. With an average HOH angle of 100.3°, a dipole moment of 2.00 D (1 D = 3.3356×10^{-30} Cm) results for both water subsystems. These values for the $BeCl_2$ solution are in the limits of error the same as those found for the $CaCl_2$ solution [4]. A comparison with the data from the simulation of the $MgCl_2$ solution would not be helpful as the intramolecular part of the water potential was different from that used here and for the $CaCl_2$ solution. As the intermolecular part of the water-water potential was the same in all three simulations the comparisons performed above are justified.

There exists a significant difference in the water molecule geometry between bulk water and hydration water of Be^{2+}. The average O–H distance increases to 0.994 Å and the HOH angle decreases to 96.9°, resulting in a dipole moment of 2.11 D. For the water molecules in the first hydration shell of Ca^{2+} the corresponding values were found to be 0.992, 96.4° and 2.12 D. Considering the big difference in size between Be^{2+} and Ca^{2+} the changes in the water molecule geometry are unexpectedly small.

5. Concluding Remarks

The MD simulation of the 1.1 molal $BeCl_2$ aqueous solution demonstrated an octahedral coordination of water molecules around Be^{2+}, which is inconsistent with the results obtained from previous spectroscopic studies. The pair distribution functions revealed a more structured first hydration shell of Be^{2+}, as compared with those of Mg^{2+} and Ca^{2+}, which is reasonable from their ionic size. The consistency between the structure functions, as well as the radial distribution functions, from the simulation and X-ray diffraction was satisfactory. However, it would not be straightforward to conclude that the hydration shell structure of Be^{2+} is reproduced correctly by the simulation, since its contribution to the total structure function is small and almost negligible for the 1.1 molal solution. The geometry of the water molecules in the first hydration shell of Be^{2+} was not deformed as much as expected in the solution, in which the water molecules dissociate due to the hydrolysis of the Be^{2+} in the real system. Thus, further improvement may be required for water potentials when they are applied to a system in which more electron transfer between ion and water molecules becomes significant. X-Ray scattering data of the 5.3 molal solution gave the average coordination number of four for Be^{2+}, consistent with the previous results. The average number of water molecules around Cl^- is about seven in the 1.1 molal solution, but decreases to about 3.5 in the 5.3 molal solution.

Acknowledgements

This work was supported by the International Collaboration Program between the Deutsche Forschungsgemeinschaft and the Japan Society for Promotion of Sciences and partly by the Grant-in-Aid for Special Project Research No. 60129031 from the Ministry of Education, Science and Culture. For part of the calculations the HITAC 200-H computers at the Institute for Molecular Science at Okazaki and the National Laboratory for High Energy Physics at Tsukuba were used. The other part of the calculations was performed on the Cray I at the computer centre of the Max-Planck-Institut für Plasmaphysik in Garching.

[1] K. Heinzinger, Pure Appl. Chem. **57,** 1031 (1985); Physica **131 B,** 196 (1985).
[2] W. Dietz, W. O. Riede, and K. Heinzinger, Z. Naturforsch. **37 a,** 1038 (1982).
[3] G. Pálinkás, T. Radnai, W. Dietz, Gy. I. Szász, and K. Heinzinger, Z. Naturforsch. **37 a,** 1049 (1982).
[4] (a) M. M. Probst, T. Radnai, K. Heinzinger, P. Bopp, and B. M. Rode, J. Phys. Chem. **89,** 753 (1985). (b) G. Pálinkás and K. Heinzinger, Chem. Phys. Lett. **126,** 251 (1986).
[5] I. G. Dance and H. C. Freeman, Acta Cryst. **B 25,** 304 (1969).

[6] S. K. Sikka and R. Chidambaram, Acta Cryst. **B 25,** 310 (1969).
[7] C. Pigenet, J. Raman Spectrosc. **13,** 66 (1982).
[8] R. E. Connick and D. N. Fiat, J. Chem. Phys. **39,** 1349 (1963).
[9] M. Alei, Jr. and J. A. Jackson, J. Chem. Phys. **41,** 3402 (1964).
[10] T. J. Swift and W. G. Sayre, J. Chem. Phys. **44,** 3567 (1966).
[11] A. Fratiello, R. E. Lee, V. M. Nishida, and R. E. Schuster, J. Chem. Phys. **48,** 3705 (1968).
[12] V. A. Sipachev and A. I. Grigor'ev, Russ. J. Struct. Chem. **10,** 710 (1969).
[13] D. J. Gardiner, R. E. Hester, and E. Mayer, J. Mol. Struct. **22,** 327 (1974).
[14] F. Bertin and J. Derouault, Comp. Rend. **c 280,** 973 (1975).
[15] S. Ishiguro, M. Maeda, S. Ono, and H. Kakihama, Denki Kagaku **46,** 553 (1978).
[16] H. Kakihama and L. G. Sillén, Acta Chem. Scand. **10,** 985 (1956).
[17] H. Tsukuda, T. Kawai, M. Maeda, and H. Ohtaki, Bull. Chem. Soc. Japan **48,** 1691 (1975).
[18] W. B. Streett, D. J. Tildesley, and G. Saville, ACS Symposium Series **86,** 144 (1978).
[19] F. H. Stillinger and A. Rahman, J. Chem. Phys. **68,** 666 (1978).
[20] P. Bopp, G. Jancsó, and K. Heinzinger, Chem. Phys. Lett. **98,** 129 (1983).
[21] G. Jancsó and P. Bopp, Z. Naturforsch. **38 a,** 206 (1983).
[22] G. H. F. Diercksen, W. P. Kramer, and B. O. Roos, Theor. Chim. Acta (Berl) **36,** 249 (1975).
[23] T. H. Dunning, J. Chem. Phys. **53,** 2823 (1970).
[24] G. Corongiu and E. Clementi, J. Chem. Phys. **69,** 4885 (1978).
[25] K. A. Kollman and I. D. Kuntz, J. Amer. Chem. Soc. **94,** 9236 (1972).
[26] H. Ohtaki, M. Maeda, and S. Itoh, Bull. Chem. Soc. Japan **47,** 2217 (1974); H. Ohtaki, T. Yamaguchi, and M. Maeda, Bull. Chem. Soc. Japan **49,** 701 (1976).
[27] T. Yamaguchi, G. Johansson, B. Holmberg, M. Maeda, and H. Ohtaki, Acta Chem. Scand. **A 38,** 437 (1984).
[28] International Tables for X-Ray Crystallography, Vol. IV, Kynoch Press, Birmingham 1974.
[29] G. Johansson and M. Sandström, Chem. Scr. **4,** 195 (1973).
[30] A. H. Narten, M. D. Danford, and H. A. Levy, Discuss. Faraday Soc. **43,** 97 (1967).
[31] T. Yamaguchi, Doctral Thesis, Tokyo Institute of Technology, 1978.
[32] H. Ohtaki and K. Yamasaki, Bull. Chem. Soc. Japan **31,** 6 (1958).
[33] R. D. Shannon, Acta Cryst. **A 32,** 751 (1976).
[34] G. Pálinkás, W. O. Riede, and K. Heinzinger, Z. Naturforsch. **32 a,** 1137 (1977).
[35] K. Heinzinger and P. C. Vogel, Z. Naturforsch. **31 a,** 363 (1976).
[36] J. E. Enderby and G. W. Neilson, Advan. Phys. **29,** 323 (1980).
[37] P. Bopp, I. Okada, H. Ohtaki, and K. Heinzinger, Z. Naturforsch. **40 a,** 116 (1985).
[38] S. Biggin, J. E. Enderby, R. L. Hahn, and A. H. Narten, J. Phys. Chem. **88,** 3634 (1984).
[39] A. P. Copestake, G. W. Neilson, and J. E. Enderby, J. Phys. C: Solid State Phys. **18,** 4211 (1985).